Journal of Ovonic Research Vol. 20, No. 3, May - June 2024, p. 395 - 403

Improvement of DC and RF characteristics for a novel AlGaAs/InGaAs HEMT with decreased single event effect

K. Xu[a], H. Y. Wang[b,*], E. L. Chen[c], S. X. Sun[c], H. L. Wang[a], H. Y. Mei[c,d]
[a]*School of Material Science and Engineering, Zhengzhou University of Aeronautics, Zhengzhou 450015, China*
[b]*Henan Key Laboratory of Smart Lighting, School of Electronic Information and Engineering, Jilin University, Changchun, 130015, China*
[c]*School of Electronic Information, Huanghuai University, Zhumadian 463000, China*
[d]*Key Laboratory of Functional Materials and Devices for Informatics of Anhui Educational Institutions, Fuyang Normal University, Fuyang, 236037*

In order to promotion the RF performance, a grade $In_{1-x}Ga_xAs$ channel (G-HEMT) introduced to the AlGaAs/InGaAs HEMT. The G-HEMT with the grade $In_{1-x}Ga_xAs$ channel forms a deeper potential well and confines more electrons in the channel, results in improving the DC and RF characteristics. Moreover, because of the grade $In_{1-x}Ga_xAs$ is effectively reduced the peak electric field, and leads to a significant increase in breakdown voltage (BV). Moreover, the G-HEMT also increases resistance to single event effects (SEE). The simulation results indicate that the f_{max} is significantly increased to 889 GHz of G-HEMT from 616 GHz of conventional AlGaAs/InGaAs HEMT (C-HEMT). The the f_T is significantly increased to 521 GHz of G-HEMT from 326 GHz of C-HEMT, as well as the I_{Dsat} is increased by 64.8% and the BV increases by 37%. In addition, the SEE peak drain current of G-HEMT is dramatically reduced 51%.

(Received April 5, 2024; Accepted June 12, 2024)

Keywords: AlGaAs/InGaAs HEMT, Grade $In_{1-x}Ga_xAs$ channel, DC and RF characteristics, Single event effect

1. Introduction

With the demand of the communications industry, it brings forward the higher request to the running speed of microelectronic devices. Owing to the high two-dimension electron gas (2DEG) density and high electron peak drift velocity, the high electron mobility transistors (HEMTs) are promising in high-speed data transmission, microwave and millimeter wave integrated circuits applications[1-3]. Among these HEMTs, AlGaAs/InGaAs HEMT shows the low noise, high gain, high frequency characteristics, which is attributed to the greater current density

* Corresponding author: 2863360340@qq.com
K. Xu and H. Y. Wang contributed equally to this work.
https://doi.org/10.15251/JOR.2024.203.395

and electron mobility for InGaAs channel[4-6]. Therefore, it is the most suitable for deep space communication, THz transmitters and receivers applications[7-9].

In order to further enhance the performance of AlGaAs/InGaAs HEMT, the different structures and manufacturing technologies have been put forward[10-13]. Lin et al.[12] studied the effect of the SiN_X-passivated on the maximum extrinsic transconductance, breakdown voltage and cutoff frequency for AlGaAs/InGaAs HEMT. The results show that the characteristics of device are improved after SiN_X-passivation due to the . Cho et al.[13] were used the double-gate supported passivation scheme to enhance the DC and RF characteristics for AlGaAs/InGaAs HEMT. Hence, the performance of the device can be improved by using different structures.

Moreover, for the AlGaAs/InGaAs HEMT applied in space communication equipment, the characteristics of device will degrade induced by the space irradiation particle[14-15]. Single event effect (SEE) is an important radiation effect[16]. However, few investigations study the SEEs on AlGaAs/InGaAs HEMT. As a result, an effective method can increase the RF characteristics simultaneously with an improved SEE, which is of great value.

In this study, a RF improved structure by adopting a grade $In_xGa_{1-x}As$ channel (G-HEMT) is proposed. The results show that the 521 GHz and 889 GHz of f_T and f_{max} for G-HEMT are achieved, which are 46.3% and 44.3% higher than that of conventional AlGaAs/InGaAs HEMT (C-HEMT). Compared with the C-HEMT, the peak value of SEE drain current (I_{peak}) for G-HEMT is lower 51% than the C-HEMT. Therefore, the G-HEMT can effectively enhance the RF characteristics and restrain SEE simultaneously.

2. Simulation details

The structure of proposed the G-HEMT is illustrated in Fig. 1 (a). The mainly characteristic for G-HEMT introduces a grade $In_{1-x}Ga_xAs$ channel , which x is ranged from 0 to 0.75, as shown in Fig. 1 (b). The separation between source electrode and drain electrode is 1.5 μm. The gate is located the center of the source-drain electrode, and set as 0.25 μm. The 2DEG concentration of 5×10^{12} cm^{-2} is set in the simulation. The more structure parameters of the device are illustrated in Table 1.

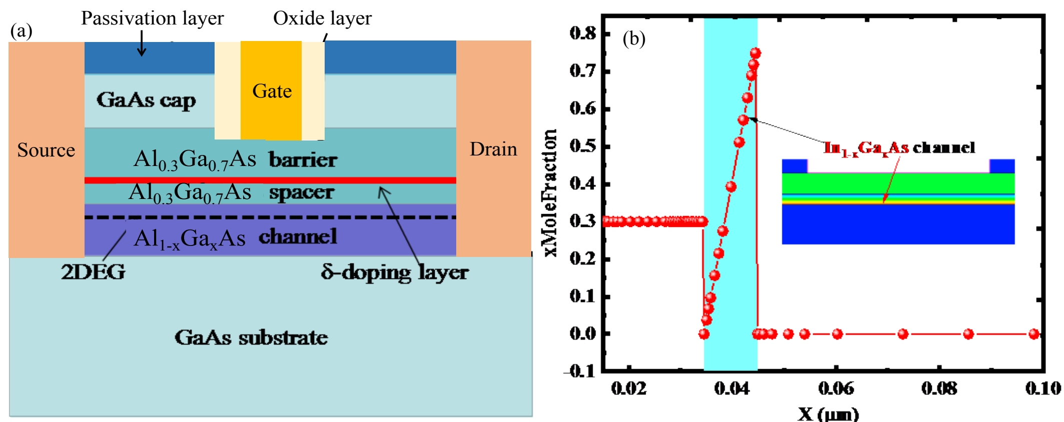

Fig. 1. (a) Structure of proposed the G-HEMT, (b) variation of mole fraction for $In_{1-x}Ga_xAs$ channel.

Table 1. Parameters for the G-HEMT.

Layer	Thickness
Passivation layer	100 nm
Oxide layer	40 nm
GaAs cap layer	30 nm
$Al_{0.3}Ga_{0.7}As$ barrier layer	31 nm
$Al_{0.3}Ga_{0.7}As$ spacer layer	3.5 nm
$In_xGa_{1-x}As$ channel layer	10 nm
GaAs substrate	800 nm

In order to simulating the carrier transport in the device, the Hydrodynamic model (HD) is used[17]. To simulating the doping dependent mobility, the DopingDenpendence model is adopted. To simulating the high field dependent mobility, the HighFieldSaturation model is adopted. For considering the recombination process, the SRH Recombination model, Auger model and Radiative model are adopted. Impact-ionization model is used to simulate the breakdown characteristic[18]. The parameters materials is described in Ref 19-20.

3. Results and discussion

3.1. DC and RF characteristics of G-HEMT

Figure 2 shows the I_{DS}–V_{GS} of G-HEMT and C-HEMT under V_{DS} of 1.5 V. Compared with the drain current (I_{DS}) and transconductance (g_m) of C-HEMT, a significant increase is obtained in the G-HEMT. It can be concluded that the grade $In_{1-x}Ga_xAs$ channel has a larger contribution to the improvement in transfer characteristics. The maximum transconductance ($g_{m,max}$) of G-HEMT is increased to 830 mS/mm from 559 mS/mm of C-HEMT, which is increased by 48.5%. The maximum drain current (I_{DS}) of G-HEMT at V_{GS}=0.5 V is increased to 930 mA/mm from 475 mA/mm of C-HEMT, which is increased by 95.8%. This is mainly because the number of carriers increases in grade $In_{1-x}Ga_xAs$ channel.

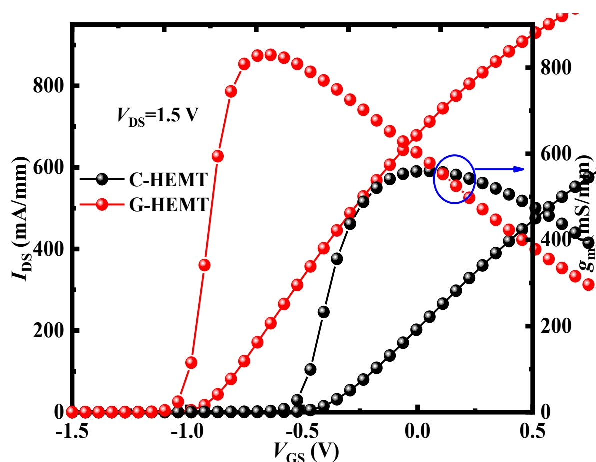

Fig. 2. I_{DS}–V_{GS} curves of to devices.

The electron concentration and energy band for G-HEMT and C-HEMT are displayed in Fig. 3. The peak electron concentration increases obviously to 2.53×10^{19} cm^{-3} for G-HEMT from 1.68×10^{19} cm^{-3} for C-HEMT, as displayed in Fig. 3 (a). A deeper potential well is formed for G-HEMT when the grade $In_{1-x}Ga_xAs$ channel is adopted, as shown in Fig 3 (b). Hence, the grade $In_{1-x}Ga_xAs$ structure confines more electrons in the channel region and lead to the G-HEMT has the higher I_{DS} and g_m.

Moreover, the threshold voltage (V_{th}) is moved from -0.45 V for C-HEMT to -0.9 V for G-HEMT. The threshold voltage of HEMT can be described by[21]: $V_{th} = \Phi_B + \frac{E_{F0}}{q} - \frac{\Delta E_C}{q} - \frac{q\times n\times d}{\varepsilon}$, where Φ_B is Schottky barrier height, E_{F0} and ΔE_C are the Fermi level and conduction band difference, respectively. d is the distance from gate to channel. n is the electron density. It can be seen that an increase of n caused by the grade $In_{1-x}Ga_xAs$ channel, as shown in Fig. 3 (a), will led to a negatively movement.

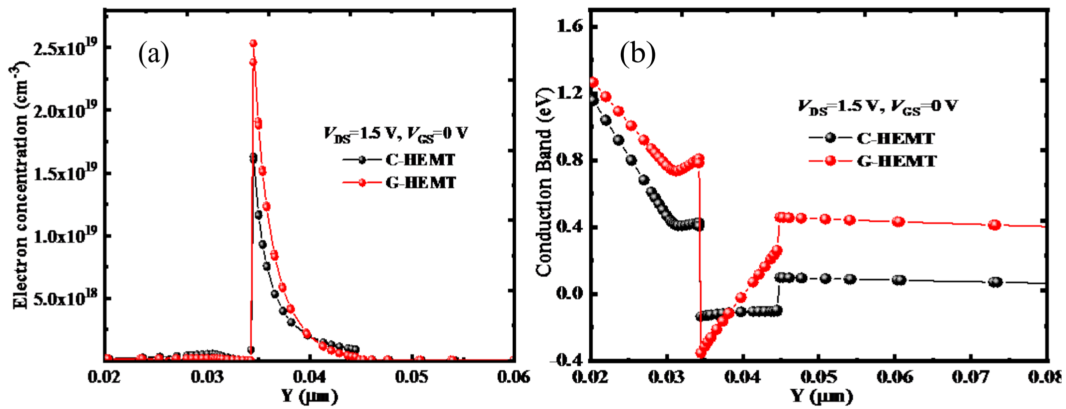

Fig. 3. (a) Electron concentration and (b) conduction band of G-HEMT and C-HEMT.

Fig. 4 shows comparison of output characteristics (I_{DS}–V_{DS}) of G-HEMT and C-HEMT. The V_{GS} is ranged from 1 to -4 V with step -1 V. The results show that the I_{DS} increases dramatically when the grade $In_{1-x}Ga_xAs$ channel is used. At V_{GS}=0.4 V, the C-HEMT exhibits the saturated channel currents (I_{Dsat}) of 421 mA/mm, where as G-HEMT exhibits a I_{Dsat} of 694 mA/mm. G-HEMT shows 64.8% improvement in I_{Dsat} compared to C-HEMT, which indicates the grade $In_{1-x}Ga_xAs$ channel does significantly improvement the output characteristics of the device. Extracted the on-resistance (R_{on}) from output curves under V_{GS}=0.4 V is shown in Fig. 4. By contrast, the G-HEMT with a grade $In_{1-x}Ga_xAs$ channel exhibits reduced R_{on} nearly 23.2%. The higher I_{Dsat} and lower R_{on} are largely due to the higher electron concentration at the interface of $AlGaAs/In_{1-x}Ga_xAs$.

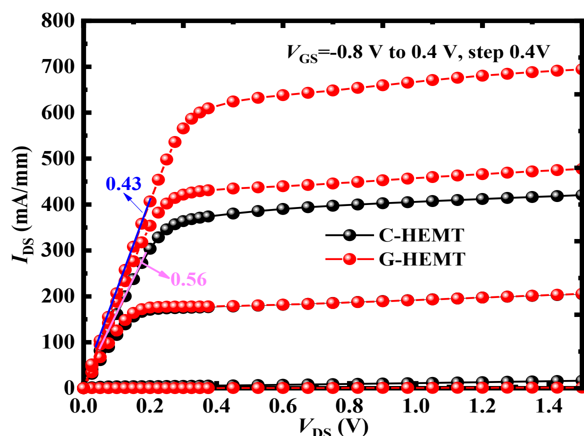

Fig. 4. I_{DS}-V_{DS} curves of two devices.

The off state breakdown voltage (*BV*) of G-HEMT and C-HEMT are also investigated. Fig. 5 (a) shows the comparison of *BV* curves on G-HEMT and C-HEMT. The BV of G-HEMT and C-HEMT are 7.3 V and 4.6 V, respectively. Therefore, the BV of G-HEMT is higher 37% than that of C-HEMT. To better understanding for the higher BV of the G-HEMT, a detailed investigation of electronic field is performed. The peak of electric field A is reduced. Moreover, the larger average electronic field at the gate-drain region is achieved by introducing the grade $In_{1-x}Ga_xAs$ channel. Therefore, the G-HEMT has the higher BV.

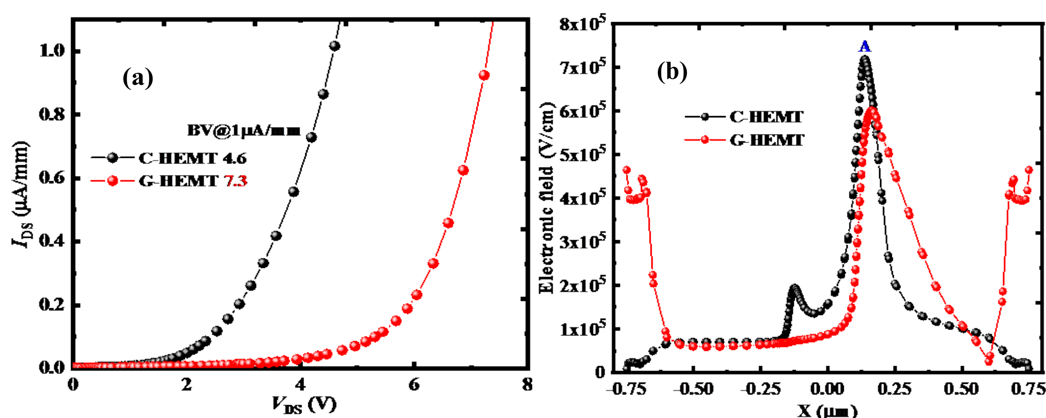

Fig. 5. (a) BV and (b) channel electric field at breakdown for two devices.

The curves of f_T and f_{max} for G-HEMT and C-HEMT are displayed in Fig. 6. The results show that the f_T and f_{max} are obviously increase for G-HEMT. The maximum f_T and f_{max} of 521 GHz and 889 GHz for G-HEMT which is comparatively 46.3% and 44.3% higher than the C-HEMT which are 356 GHz and 616 GHz. The dramatically increased f_T and f_{max} for G-HEMT is mainly due to the increase of the transconductance. Additionally, the grade $In_{1-x}Ga_xAs$ channel increases the number of electrons in channel, resulting in decrease of the channel resistance, and lead to improving the f_T and f_{max}.

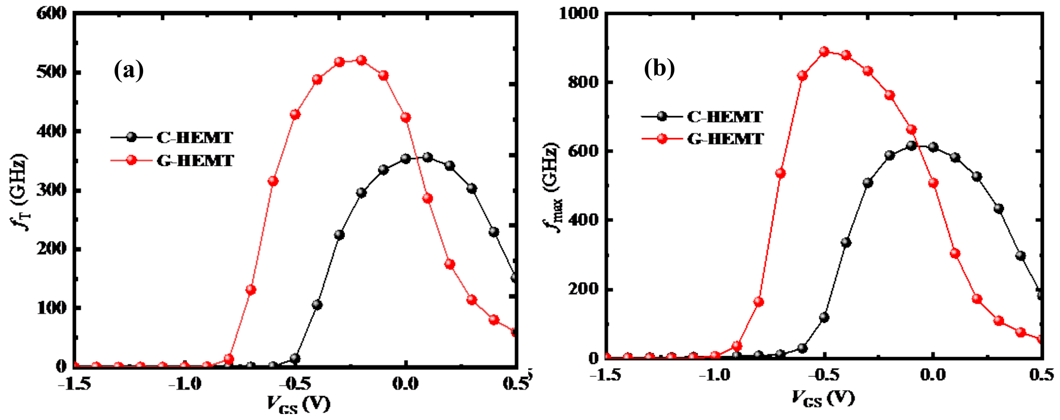

Fig. 6. Variation of (a) f_T and (b) f_{max} for G-HEMT and C-HEMT.

3.2. Single event effect

In this part, the variation of I_{DS} induced by single event effect for the G-HEMT and C-HEMT is studied. The electron-hole pairs generation rate along the ion trajectory can be described by[22]:

$$\mathrm{Rate}(x,y)=\frac{\mathrm{LET}}{q\pi\omega_0 T_\mathrm{C}}\exp\left(-\frac{(x-x_0)^2}{\omega_0^2}\cdot\exp\left(-\frac{(t-T_0)^2}{T_\mathrm{C}^2}\right)\right)$$

where, the track radius ω_0 is set as 0.02 μm. The LET of 0.5 pC/μm is set in simulation . T_0 is set as 1×10^{-11} s and T_C is set as 2×10^{-12} s.

In this study, the ion is vertical access and across the entire device. The incidence position is set as the center of gate. Fig. 7 shows the curves of I_{DS} for G-HEMT and C-HEMT at V_{DS}=0.5 V and V_{GS}=-1.5 V. The results indicate that the I_{DS} for two devices are increased rapidly firstly and reached to the peak value (I_{peak}), then fell sharply. However, the I_{peak} of G-HEMT has a 51 % lower I_{peak} than that C-HEMT. Hence, the G-HEMT shows the better resistance to single event effect than the C-HEMT.

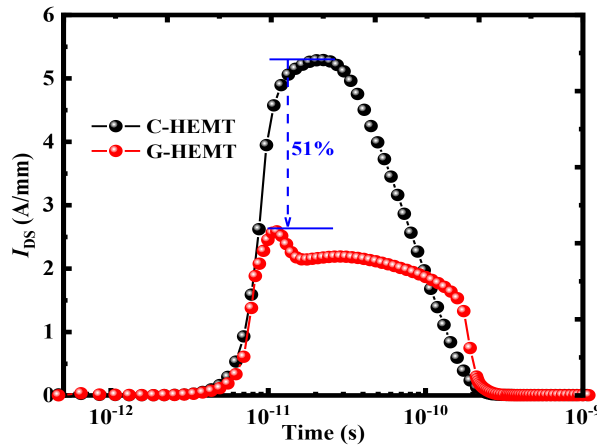

Fig. 7. Variation of I_{DS} for G-HEMT and C-HEMT atV_{DS} = 0.5 V and V_{GS} =-1.5 V.

To understand the causes of the lower I_{peak} for G-HEMT, the variation of electronic field is

analyzed, as shown in Fig. 8 (a). The time to obtain the electric field is the peak time (T_{peak}). Compared with the C-HEMT, the smaller value of electric field is obtained for G-HEMT, especially near the gate. The lower electric field will lead to the lower impact ionization rate (IR). For C-HEMT, the IR is 10^{28} $cm^{-3}s^{-1}$ near the gate at T_{peak}. For G-HEMT, the IR is 10^{26} $cm^{-3}s^{-1}$ near the gate at T_{peak}, which is much lower the C-HEMT. Therefore, the less electrons produces for G-HEMT at T_{peak}, and thus greatly lowers the I_{peak}.

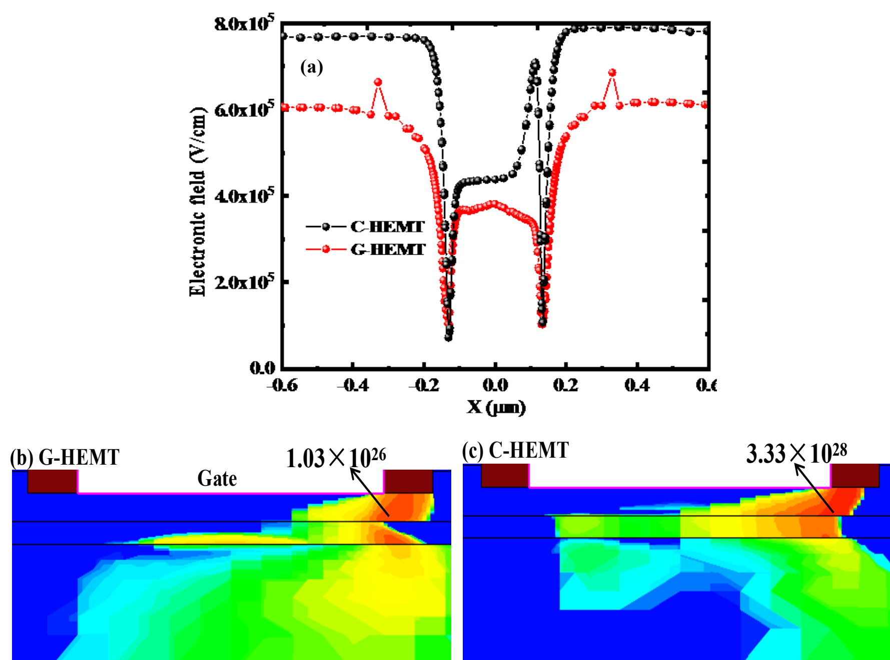

Fig. 8 (a) Electric field distribution, (b) and (c) impact ionization rate for G-HEMT and C-HEMT.

4. Conclusions

In this study, a high performance G-HEMT with a grade $In_{1-x}Ga_xAs$ channel is proposed to improve the DC and RF characteristics. Owing to the grade $In_{1-x}Ga_xAs$ channel, the deeper potential well is formed between spacer layer and channel layer, result in increasing the number of electrons in the grade $In_{1-x}Ga_xAs$ channel. Therefore, the $g_{m,max}$, I_{Dsat}, f_T and f_{max} of the G-HEMT are higher 48.5%, 64.8%, 46.3% and 44.3% than that of C-HEMT. Moreover, the electric field distribution is also modulated by adopting the grade $In_{1-x}Ga_xAs$ channel, the BV and SEE are also improved. The BV of the G-HEMT is increased to 7.5 V from the 4.7 V, which is increased by 37%. Meanwhile, the $I_{peak}$is reduced to 51% for G-HEMT.

Acknowledgements

This work was supported by Major Science and Technology Project of Zhumadian City Grant ZMDSZDZX2022004, Henan Province Joint Fund Project of Science and Technology under Grant 225200810085, Henan Provincial Science and Technology Research Project under Grant 232102210173, 232102311204, Henan Key Laboratory of Smart Lighting Grant 2023KF07,

Zhumadian City Science and Technology Innovation Youth Project QNZX202325, Open Project of Provincial and Ministerial Scientific Research Platform, Fuyang Normal University (NO.FSKFKT015D).

References

[1] A. Fargi, S. Ghedira, A. Kalboussi, AIP Adv. 13, 105016 (2023); https://doi.org/10.1063/5.0167563

[2] S. Bhattacharya, J. Ajayan, D.Nirmal, S. Tayal, S. Kollem, L. M. I. Leo Joseph, Silicon 14, 9581-9588 (2022); https://doi.org/10.1007/s12633-022-01719-2

[3] J. Ajayan, T. Ravichandran, P. Mohankumar, P. Prajoon, J. Charles Pravin, D. Nirmal, IETE J. Res. 67, 366-376 (2021).

[4] C. C. Cheng, C. C. Wu, Y. T. Fan, J. S. Wu, S. D. Lin, AIP Adv. 8, 095029 (2018); https://doi.org/10.1063/1.5040382

[5] Y. S. Lin, J. J. Huang, J. Korean Phys. Soc. 79, 828-831 (2021); https://doi.org/10.1007/s40042-021-00299-5

[6] X. Y. Luo, A. O'Hara, X. Li, P. F. Wang, E. X. Zhang, R. D. Schrimpf, S. T. Pantelides, D. M. Fleetwood, J. Appl. Phys. 135, 025702 (2024); https://doi.org/10.1063/5.0187747

[7] M. Abdul Alim, A. Jarndal, C. Gaquiere, G. Crupi, J Mater Sci: Mater Electron 34, 892 (2023); https://doi.org/10.1007/s10854-023-10176-5

[8] J. H. Tsai, P. S. Lin, Y. C. Chen, S. H. Liou, J. S. Niu, Semiconductors 53, 406-410 (2019); https://doi.org/10.1134/S1063782619030187

[9] J. Ajayan, D. Nirmal, P. Mohankuma, D. Kuriyan, A.S. Augustine Fletche, L. Arivazhagan, B. S. Kumar, Microelectron. J. 92, 104604 (2019); https://doi.org/10.1016/j.mejo.2019.104604

[10] E. A. Tarasova, S. V. Khazanova, O. L. Golikov, A. S. Puzanov, S. V. Obolensky, V. E. Zemlyakov, Semiconductors 55, 895-898 (2021); https://doi.org/10.1134/S1063782621100250

[11] S. R Panda, M. Pradhan, T. Sahu, A. K. Panda, Phys. Scr. 98, 125984 (2023); https://doi.org/10.1088/1402-4896/ad0934

[12] Y. S. Lin, B. Y. Chen, Microelectron. Eng. 214, 100-103 (2019); https://doi.org/10.1016/j.mee.2019.04.028

[13] S. J. Cho, C. Wang, N. Y. Kim, Microelectron. Eng. 113, 11-19 (2014); https://doi.org/10.1016/j.mee.2013.07.001

[14] H. L. Wang, S. X. Sun, H. Y. Mei, Y. T. Gao, J. Ovonic Res. 19, 483-491 (2023); https://doi.org/10.15251/JOR.2023.195.483

[15] A. N. Klochkov, A. Yskakov, A. N. Vinichenko, D. A. Safonov, N. I. Kargin, M. V. Bulavin, A. V. Galushko, V. R. Yamurzin, I. S. Vasil'evskii, Materials 16, 6750 (2023); https://doi.org/10.3390/ma16206750

[16] S. Sun, X. Xie, P. Zhang, Z. Zhao, J. Wei, X. Luo, J. Sci.: Adv. Mater. Dev. 9, 100692 (2024); https://doi.org/10.1016/j.jsamd.2024.100692

[17] J. Ajayan, T. Ravichandran, P. Mohankumar, P. Prajoon, J. Charles Pravin, D. Nirmal, Int. J. Electron. Commun. (AEÜ) 84, 387-393 (2018);

https://doi.org/10.1016/j.aeue.2017.12.022

[18] J. F. Du, R. N. Li, Z. Y. Bai, Y. Liu, Q. Yu, Superlatt. Microstruct. 111, 760-766 (2017); https://doi.org/10.1016/j.spmi.2017.07.033

[19] S. X. Sun, L. H. Ma, C. Cheng, C. Zhang, Y. H. Zhong, Y. X. Li, P. Ding, Z. Jin, Phys. Status Solidi A 214, 1700322 (2017); https://doi.org/10.1002/pssa.201700322

[20] J. Ajayan, D. Nirmal, Superlatt. Microstruct. 100, 526-534 (2016); https://doi.org/10.1016/j.spmi.2016.10.011

[21] Y. Chen, L. A. Yang, H. B. Yue, Y. C. Liu, Z. Jin, Y. B. Su, Y. Hao, IEEE Trans. Electron Devices 69, 988-993 (2022); https://doi.org/10.1109/TED.2022.3144118

[22] J. C. Zhou, Y. Wang , X. J. Li, J. Q. Yang, M. T. Bao, F. Cao, IEEE Trans. Electron Devices 69, 3283-3289 (2022); https://doi.org/10.1109/TED.2022.3166122